Original Article

Differential chondro- and osteo-stimulation in three-dimensional porous scaffolds with different topological surfaces provides a design strategy for biphasic osteochondral engineering

Chinmaya Mahapatra[1,2], Jung-Ju Kim[1,2], Jung-Hwan Lee[1,2,3,4], Guang-Zhen Jin[1,2,4], Jonathan C Knowles[1,4,5] and Hae-Won Kim[1,2,4] iD

Abstract

Bone/cartilage interfacial tissue engineering needs to satisfy the differential properties and architectures of the osteochondral region. Therefore, biphasic or multiphasic scaffolds that aim to mimic the gradient hierarchy are widely used. Here, we find that two differently structured (topographically) three-dimensional scaffolds, namely, "dense" and "nanofibrous" surfaces, show differential stimulation in osteo- and chondro-responses of cells. While the nanofibrous scaffolds accelerate the osteogenesis of mesenchymal stem cells, the dense scaffolds are better in preserving the phenotypes of chondrocytes. Two types of porous scaffolds, generated by a salt-leaching method combined with a phase-separation process using the poly(lactic acid) composition, had a similar level of porosity (~90%) and pore size (~150 μm). The major difference in the surface nanostructure led to substantial changes in the surface area and water hydrophilicity (nanofibrous >> dense); as a result, the nanofibrous scaffolds increased the cell-to-matrix adhesion of mesenchymal stem cells significantly while decreasing the cell-to-cell contracts. Importantly, the chondrocytes, when cultured on nanofibrous scaffolds, were prone to lose their phenotype, including reduced chondrogenic expressions (SOX-9, collagen type II, and Aggrecan) and glycosaminoglycan content, which was ascribed to the enhanced cell–matrix adhesion with reduced cell–cell contacts. On the contrary, the osteogenesis of mesenchymal stem cells was significantly accelerated by the improved cell-to-matrix adhesion, as evidenced in the enhanced osteogenic expressions (RUNX2, bone sialoprotein, and osteopontin) and cellular mineralization. Based on these findings, we consider that the dense scaffold is preferentially used for the chondral-part, whereas the nanofibrous structure is suitable for osteo-part, to provide an optimal biphasic matrix environment for osteochondral tissue engineering.

Keywords

Biphasic scaffolds, nanofibrous surface, dense surface, chondrocyte maintenance, osteogenesis, matrix adhesion, cell–cell contact, osteochondral engineering

Date Received: 31 August 2018; accepted: 7 January 2019

[1]Institute of Tissue Regeneration Engineering (ITREN), Dankook University, Cheonan, Republic of Korea
[2]Department of Nanobiomedical Science and BK21 PLUS NBM Global Research Center for Regenerative Medicine, Dankook University, Cheonan, Republic of Korea
[3]Department of Biomaterials Science, School of Dentistry, Dankook University, Cheonan, Republic of Korea
[4]UCL Eastman-Korea Dental Medicine Innovation Centre, Dankook University, Cheonan, Republic of Korea

[5]Division of Biomaterials and Tissue Engineering, UCL Eastman Dental Institute, London, UK

Corresponding author:
Hae-Won Kim, Department of Nanobiomedical Science and BK21 PLUS NBM Global Research Center for Regenerative Medicine, Dankook University, Cheonan 330-714, Republic of Korea.
Email: kimhw@dku.edu

Introduction

Current clinical treatments of the damaged osteochondral tissues, including abrasion arthroplasty, chondral shaving, and mosaicplasty, have experienced significant challenges due to the donor site morbidity, implant loss, and limited durability.[1–4] Tissue engineering approach can thus offer a solution to this, where biocompatible scaffolds combined with cells and bioactive molecules can recapitulate the tissue environments and ultimately restore the functions of damaged osteochondral tissues.[5] However, the complete regeneration of the osteochondral tissues has been difficult mainly due to the complexity of the tissue structure, cell type, and biomechanical properties.[6–9] Among the tissue engineering components, scaffolds play a key role, providing three-dimensional (3D) environments for cells to properly proliferate and differentiate.[1,10–13] Strategies for the design of osteochondral scaffolds are mainly focused on the use of biphasic or multiphasic scaffolds that combine different material compositions or physical structures to ideally recruit and populate each cell type required.[11–13]

The osteo-part of the biphasic scaffolds generally uses synthetic polymers that are combined with bioactive inorganic phases, which is known to enhance the osteogenic potential of mesenchymal stem cells (MSCs).[11,14,15] For instance, the polymeric scaffolds incorporated or coated with mineralized phase were shown to stimulate the osteogenic differentiation of MSCs.[10] Furthermore, tailoring the surface topology of the scaffolds by increasing the roughness or the use of nano-scaled matrices like nanofibers resulted in better cell adhesion to the matrix, followed by subsequently elongated cell morphology and stimulated osteogenic commitment of stem cells.[16–18] Therefore, the scaffolds for osteo-part need a proper combination of the composition and architecture that is able to provide optimal matrix conditions for enhanced osteogenesis of cells.

On the contrary, the chondral region of the osteochondral scaffolds needs a completely different approach. Cell condensation and aggregation is the required step to chondrogenesis and also accounts for the maintenance of the chondrocyte (CC) phenotype.[19] In order to enhance the cell-to-cell contact, several works focused on the preparation of cell constructs using the pellet culture methods which were free of scaffolds.[20–22] However, the low stability of the constructs and the necrosis in the central areas are considered to be a major limitation for their potential applications.[23] For this reason, the 3D scaffolding matrices are in great need to cultivate cells for chondrogenesis or to maintain the phenotype of CCs.[23–25] Some of the previous works have demonstrated the importance of the pore size of the scaffolds that is proper to culture CCs and to preserve the phenotype expressions.[26,27] Others reported that the nanofibrous matrices were proper for the CC culture and the chondrogenic differentiation of stem cells, where though other morphologies of matrices were not compared with.[28] However, systematic studies on the preferred surfaces or matrix conditions for the stimulation of chondrogenesis or the maintenance of CCs are largely limited. Recently, Cao et al.[29] designed an experiment of culturing MSCs in different-sized microwells for chondrogenesis, wherein the expression of chondrogenic markers increased as the cell-to-cell contact was enhanced in the bigger microwells and suggested the importance of engineered cell culture conditions for chondrogenesis. It is thus likely that engineering of 3D matrices to enable better cell-to-cell contact might be a proper strategy for the development of scaffolds for chondro-part.

With these in mind, here, we focus on the unique structured scaffolds, the nanofibrous matrix. Among the considered parameters of scaffolds, such as matrix molecules, chemical group, elasticity, and pore geometry, the surface nanofibrous structure (nano topology) has been potentially studied for the repair of many tissues and thus considered a fascinating physical parameter of matrices. Although the electrospun nanofibers have been popularly studied, this class is considered to be pseudo-3D (or more like two-dimensional (2D)), thus not ideal for osteochondral scaffolds. Therefore, we develop here the nanofibrous matrix into 3D porous scaffolds by employing a salt-leaching technique in conjunction with a phase separation, as previously reported.[30] We analyze whether the nanofibrous 3D scaffolds have the potential for stimulating chondro-responses and/or osteo-responses of target cells, in direct comparison with the dense-surfaced counterpart. This study is considered to deliver some insights into the design strategy of biphasic osteo- and chondro-part of scaffolds for the cell-scaffold-based osteochondral tissue engineering.

Materials and methods

Preparation of dense- and nanofibrous-surfaced 3D scaffolds

Dense- and nanofibrous-3D scaffolds were fabricated with poly-L/D-lactide acid (PLDLA; RESOMER@LR 708; Evonik). In brief, PLDLA was dissolved at 5%w/v in a co-solvent of chloroform/1,4-dioxane (1:4). The prepared PLDLA slurry was first added to a plastic mold and then salt particles (range: $100–150\,\mu m$) were packed into the solution, which was then frozen at $-20°C$ overnight. After freeze drying, the embedded salt particles were thoroughly leached out for 3 days with distilled water (DW). In case of the nanofibrous-surfaced 3D scaffold, the camphene-assisted phase-separation method was used as reported in our previous work.[31] For this, the camphene was added into the PLDLA slurry at a ratio of 4 (camphene:PLDLA by weight). The further procedures were the same as those used for dense scaffolds as described above.

For the preparation of dense and nanofibrous double-layered scaffolds, two different PLDLA solutions were

prepared. Specifically, 5%w/v PLDLA (for dense layer) and 5%w/v PLDLA plus 10%w/v camphene (for nanofibrous layer) were dissolved separately in 10 mL of chloroform/1,4-dioxane (1:4). The PLDLA solution was first added to a mold with packed salt particles (smaller sizes of 100–150 μm). Subsequently, the PLDLA plus camphene solution was added to the same mold with packed salt particles (larger sizes of 200–500 μm), which was also frozen, freeze-dried, and salt-leached thoroughly. The double layer is easily discernable based on the different pore sizes obtained from the two different-sized salt particles.

Characterization of scaffolds

The morphology of the scaffolds was observed by scanning electron microscopy (SEM, S-3000H, Hitachi, Japan). The porosity and pore size distribution of the scaffolds were analyzed using a mercury porosimeter (PM33, Quantachrome, USA). The specific surface area was measured by the N_2 adsorption/desorption (Quantachrome) based on Brunauer–Emmett–Teller (BET) method. The water affinity of the scaffolds was tested by measuring the water contact angle using a Phoenix 300 analyzer. The water droplet images made onto the scaffold were observed using a viewing system until the equilibrium shape was achieved. Data were recorded for up to 20 min, and five samples were tested for each group. The mechanical properties of the scaffolds were determined using an Instron (Model 3344). The scaffolds were prepared by casting the polymers into a cylindrical mold ($h = 10$ mm and $\varnothing = 4$ mm). Scaffolds were tested by a compression mode with a 50-N load cell and a cross-head speed of 2 mm/min. The maximum compressive strength and elastic modulus were determined from the strain–stress curve. At least four scaffolds were tested for each group.

Isolation of cells and culture

Primary CCs and MSCs were isolated from 5-week-old Sprague Dawley rats (180–200 g) to test the chondrogenesis and osteogenesis ability on the scaffolds. The animal experiment was followed according to the guidelines approved by the Animal Care and Use Committee of Dankook University. The CCs were isolated from the resting zone of costochondral cartilage growth plate and rib region, as described elsewhere.[32] Dissected rib cages were cut into small pieces and digested in 10 mL of Dulbecco's phosphate-buffered saline (DPBS) containing 0.25% ethylenediaminetetraacetic acid (EDTA) and incubated for 20 min at 37°C. The digested pieces were then incubated in 0.25% trypsin (GIBCO, Waltham, MA, USA) for 1 h and in 0.2% collagenase type 2 for 3 h. The digested tissues were centrifuged at 2000 r/min followed by a filtration with a sterile 45 μm sieve filter (BD Biosciences, Franklin Lakes, NJ, USA). CCs were plated at a density of 2.5×10^4 cells/cm² and

cultured in Dulbecco's modified Eagle's medium (DMEM) with high glucose containing 10% fetal bovine serum (FBS), 1% penicillin/streptomycin, 50 μg/mL ascorbic acid, and 1% insulin-transferrin-sodium selenite (ITS) premix (Sigma, St. Louis, MO, USA). Third passage of confluent cells was harvested for seeding onto scaffolds.

The MSCs were obtained from bone marrow of the tibia and femoral region.[33] The harvested product was centrifuged, and the supernatant was collected and suspended within a culture flask containing a normal culture medium (α-minimal essential medium (α-MEM)) supplemented with 10% FBS, 100 U/mL penicillin, and 100 mg/mL streptomycin. After incubating for 1 day, the medium was refreshed and cultured until the cells reached near confluence. The cells were subcultured with trypsinization and maintained in normal culture conditions. Second or third passage cells were harvested for seeding on scaffolds. The two types of primary cultured cells were incubated at 37°C in a humidified atmosphere of 5% CO_2 with media changes every 2–3 days.

CC assays on scaffolds

Cell-to-scaffold adhesion and proliferation. Cell-to-scaffold interaction was examined. CCs were seeded on the scaffolds at a density of 5×10^5 cells per 3D scaffold (1 mm height $\times$ 4 mm diameter). The gene expression of Integrin β1 was confirmed by the gel-based quantitative polymerase chain reaction (qPCR). Glyceraldehyde 3-phosphate dehydrogenase (GAPDH) was used as a control. The messenger RNA (mRNA) was extracted by directly dipping the scaffolds in lysis buffer (300 μL), and complementary DNA (cDNA) was synthesized from the total extracted RNA (1 μg) using a RT-PreMix (Bioneer Ltd, Daejeon, Korea). cDNA (2 μL) was subjected to a polymerase chain reaction (PCR) amplification (Applied Biosystems Veriti Thermal Cycle) using specific designed primers (basic local alignment search tool (BLAST), National Center for Biotechnology Information (NCBI)) with pre-mixed PCR kit (Bioneer Ltd). PCR reactions were conducted using 40 cycles at 95°C for 30 s, 58°C for 30 s, and then at 75°C for 60 s. Experiments were performed in triplicate. Sample band intensity was quantified using a software program GeneTools ver. 4.01 (Syngene UK) and normalized to that of GAPDH transcripts.

The adhesive cell number was indirectly calculated by counting the unattached cell number using hemocytometer. For the cell proliferation test, the cell counting kit-8 (CCK-8; Dojindo Molecular Technologies) was used. Briefly, 2.5×10^4 cells were seeded to 3D scaffold and then cultured for 1, 3, 7, and 14 days. At each time, the samples were transferred to new 96-well plates and washed three times with phosphate-buffered saline (PBS), replacing the culture media with a working CCK-8 solution. The reagent was left to react for 2 h at 37°C and then an optical

Table 1. Primer sequences of adhesion-related genes used for RT-PCR.

Gene		Sequence
GAPDH	Forward primer	5′GGAGGAATGTAACACGACTGC3′
	Reverse primer	5′CAGATGAACTGAAGGACCACC3′
Integrin β1	Forward primer	5′ACCACAGTCCATGCCATCAC3′
	Reverse primer	5′CCACCACCCTGTTGCTGTA3′

qPCR: quantitative polymerase chain reaction; GAPDH: glyceraldehyde 3-phosphate dehydrogenase.

Table 2. Primer sequences of chondrogenesis-related genes used for qRT-PCR.

Gene		Sequence
GAPDH	Forward primer	5′CTGGAAGATGGTGATGG3′
	Reverse primer	5′GATTTGGTCGTATTGGGCG3′
Aggrecan	Forward primer	5′TCGCAAGTCCCTTCCACATC3′
	Reverse primer	5′TCAAGGCGTCCTGAAGTGTC3′
Collagen type II	Forward primer	5′GCTGGTGCACAAGGTCCTAT3′
	Reverse primer	5′AGGGCCAGAAGTACCCTGAT3′
Sox9	Forward primer	5′CCAGCAAGAACAAGCCACAC3′
	Reverse primer	5′CTTGCCCAGAGTCTTGCTGA3′

RT-PCR: reverse transcription polymerase chain reaction; GAPDH: glyceraldehyde 3-phosphate dehydrogenase.

density was measured at an absorbance 450 nm (Bio-Rad iMark reader).

Cell-to-cell interaction assays. To accurately determine the cell-to-cell contact, we prepared thin 2D films which have the same surface nano topology as the 3D scaffolds. In brief, the PLDLA slurry was prepared as described above. In case of the nanofibrous structured membrane, the camphene-added PLDLA slurry was used. The completely dissolved slurries were poured into a Teflon mold to freeze under liquid nitrogen condition and then freeze-dried for 3 days. The cell-to-cell interaction was examined by the aggregated colonies, and the number of cells at the aggregated colony region was counted. Also, the expression of collagen type II (Col II) was examined as an indication of a cell-to-cell contact of CCs. For this, 2×10^4 cells were seeded onto each 2D membrane (16 mm of diameter) for a culture period of 7 days. After this, samples were fixed in 4% paraformaldehyde (PFA) and then treated with 0.2% triton X-100. After washing with PBS, samples were treated with Alexa Fluor 546 phalloidin (Invitrogen) to stain α-actin and 4′,6-diamidino-2-phenylindole (DAPI; Invitrogen) to stain nucleus. For immunofluorescence staining, primary antibody mouse monoclonal anti-collagen type II antibody (SC-52658, 1:500) and secondary antibody rabbit anti-mouse fluorescein isothiocyanate (FITC) were used. Images were visualized under a confocal laser scanning microscope (CLSM; Zeiss 700) and analyzed by ZEN 2009 software.

Chondrogenesis of CC: gene expressions. Chondrogenesis was determined by the expression of chondral-related genes (SOX-9, COL-II, and Aggrecan) after culturing the cells in chondrogenic media for 7 and 14 days. The mRNA was isolated using RNeasy Mini Kit (Qiagen, 74106) according to the manufacturer's instructions. Reverse transcription was performed using a thermal cycler (HID Veriti®96-Well Thermal Cycler, Applied Biosystems, 4479071), and the obtained cDNA was quantified with an ultraviolet (UV)–vis spectrophotometer (NanoDrop 2000; Thermo Scientific). Gene expression level was evaluated by a real-time PCR equipment (StepOnePlus™; Applied Biosystems) using SensiMix™ SYBR Kit (Bioline, QT605). Primers for the gene amplification are summarized in Tables 1 and 2, as referenced to a previous report.[34] The PCR was initiated with an activation step of 20 s at 95°C, followed by 40 cycles of denaturation (15 s, 95°C), annealing (30 s, 60°C), and extension (30 s, 72°C), as recommended by the manufacturer. Relative gene expression levels for target genes were normalized to the endogenous GAPDH gene using comparative Ct method ($2^{-\Delta\Delta Ct}$) as previously mentioned.

Maturation of CCs. Glycosaminoglycan (GAG) production was observed by Alcian blue staining and quantitatively analyzed at 14 and 21 days. In brief, the scaffolds were rinsed with PBS followed a fixation in 4% PFA at 4°C for 10 min. The scaffolds were transferred to 1% Alcian blue (Sigma) solution, diluted in 3% acetic acid followed by an incubation at room temperature for 30 min. The scaffolds were rinsed in DW three times followed by an incubation in 1% sodium dodecyl sulfate (SDS) for 30 min to solubilize the Alcian blue stain. The absorbance of eluting solution was measured at 595 nm using iMark reader.

MSCs assays on scaffolds

Cell-to-scaffold adhesion and proliferation. The initial adhesion behavior of MSCs onto the scaffolds was investigated by counting the attached cell numbers. In brief, 5×10^5 cells were seeded onto each 3D scaffold and cultured for 2, 4, 8, and 16 h, and the number of attached cells was determined by measuring the remaining cells in the media using hemocytometer. To observe the morphology, the cells were fixed in 4% PFA for 10 min at room temperature and then permeabilized with 0.1% triton X-100 for 3 min, followed by PBS washing and then blocking with 1% bovine serum albumin (BSA) for 30 min. The cells were stained with Alexa Fluor 555 phalloidin for 45 min at room temperature followed by PBS washing, and the nuclei were stained with DAPI for 5 min, and the cell images were visualized with CLSM. For the proliferation test, the CCK-8 was used. Briefly, 2.5×10^4 cells were seeded onto each 3D scaffold and cultured for 1, 3, 7, and 14 days. The CCK assay was followed by the same protocol as mentioned above.

Osteogenesis of MSCs: protein expression. Osteogenesis of MSCs was determined by the expression of proteins related to osteoblasts (RUNX2, bone sialoprotein (BSP), and osteopontin (OPN)) by the western blot at 7 and 14 days. GAPDH was used as a control. In brief, the protein extracts from the MSCs cultured in an osteogenic medium were prepared by a radioimmunoprecipitation assay (RIPA) buffer (PRO-PREP™ Protein Extraction Solution; iNtRON, South Korea). Protein samples were resolved on 10% SDS–polyacrylamide gel by boiling at 100°C for 4 min in 2× sample buffer followed by transblotting to nitrocellulose membranes (Millipore). The membranes were blocked with 5% BSA in Tris-buffered saline with 0.1% Tween 20 and then probed with proper primary antibodies (rabbit anti-RUNX2 antibody SC-10758 at 1:500, mouse anti-OPN antibody SC-20788 at 1:500, rabbit anti-BSP antibody SC-292394 at 1:1000, and mouse anti-GAPDH antibody SC-25778 at 1:500). Secondary antibodies were goat anti-mouse and goat anti-rabbit FITC antibody. All antibodies were purchased from Santa Cruz Biotechnology, Inc. The blotted membranes were then incubated with horseradish peroxidase (HRP)-conjugated secondary immunoglobulin G (Invitrogen), and band signals were detected using enhanced chemiluminescent (ECL) detection reagent (Pierce, Rockford, USA). ECL treatment membrane was visualized using an LAS-1000 mini image analyzer (GE, USA), and the band intensities were quantitatively analyzed by ImageJ software (National Institutes of Health (NIH)).

Maturation of MSCs. As the terminal osteogenic marker, cellular mineralization was assessed by means of an Alizarin red S (ARS) staining at 28 days of culture in an osteogenic induction medium. Briefly, cells were washed with PBS and fixed with 10% PFA for 15 min at room temperature. Cells were stained with 40 mM ARS solution (pH 4.2) and incubated for 10 min at room temperature with gentle shaking. The media were aspirated and the scaffolds were washed three times. The stained samples were captured using a digital camera. For quantification, the ARS stain was de-stained using 10% cetylpyridinium chloride (CPC) in 10 mM sodium phosphate buffer (pH 7.0) for 15 min at room temperature. Aliquots of extracts were diluted 10-fold in 10% CPC solution, and an absorbance of elucidated solution was detected at 562 nm using a microplate reader.

Statistical analysis

All results are presented as means ± standard deviations. A Student's *t*-test was performed to determine the significant difference ($p < 0.05$) between groups.

Results and discussion

Characteristics of the nanofibrous- and dense-surfaced scaffolds

The physico-chemical properties of the dense- and nanofibrous-surfaced 3D scaffolds were characterized. The SEM images showed the overall morphologies of the scaffolds. Both scaffolds presented similar macroporous structures comprising interconnected pores with sizes around 100–200 μm (Figure 1(a)). A closer examination, however, revealed the significantly different internal morphologies. The phase-separation process induced by the use of camphene allowed the creation of a highly nanofibrous morphology[35] while maintaining the overall macropore configuration, whereas a smooth and dense pore morphology was produced in the absence of camphene. The total porosity of the scaffolds was not much different based on the result of mercury intrusion porosimetry; a total porosity of 89.7% and 89.0% for the dense and nanofibrous scaffold, respectively (Figure 1(b)). The pore size distribution was similar in both scaffolds, with pores mainly peaked at 100–200 μm, reflecting the SEM observation. However, the nanofibrous scaffolds also contained huge amount of inter-fiber spaces on the frameworks (submicron to a few microns) due to the nanofibrous structure, which however, might not be detected by the mercury intrusion porosimetry. The specific surface area was then measured by the nitrogen adsorption/desorption isotherms using the BET method (Figure 1(c)). Together with the specific surface area, the hydrophilicity of the scaffolds was also determined by a contact angle measurement (Figure 1(d)). The water contact angle decreased gradually with time for both scaffolds, due to the time-sequenced water permeation behavior. The nanofibrous scaffolds showed much lower contact angles than the dense scaffolds, suggesting the water molecules should react with the nanofibrous surface of scaffolds more quickly than the dense surface. Due to the higher surface area, the nanofibrous surface could provide more reaction
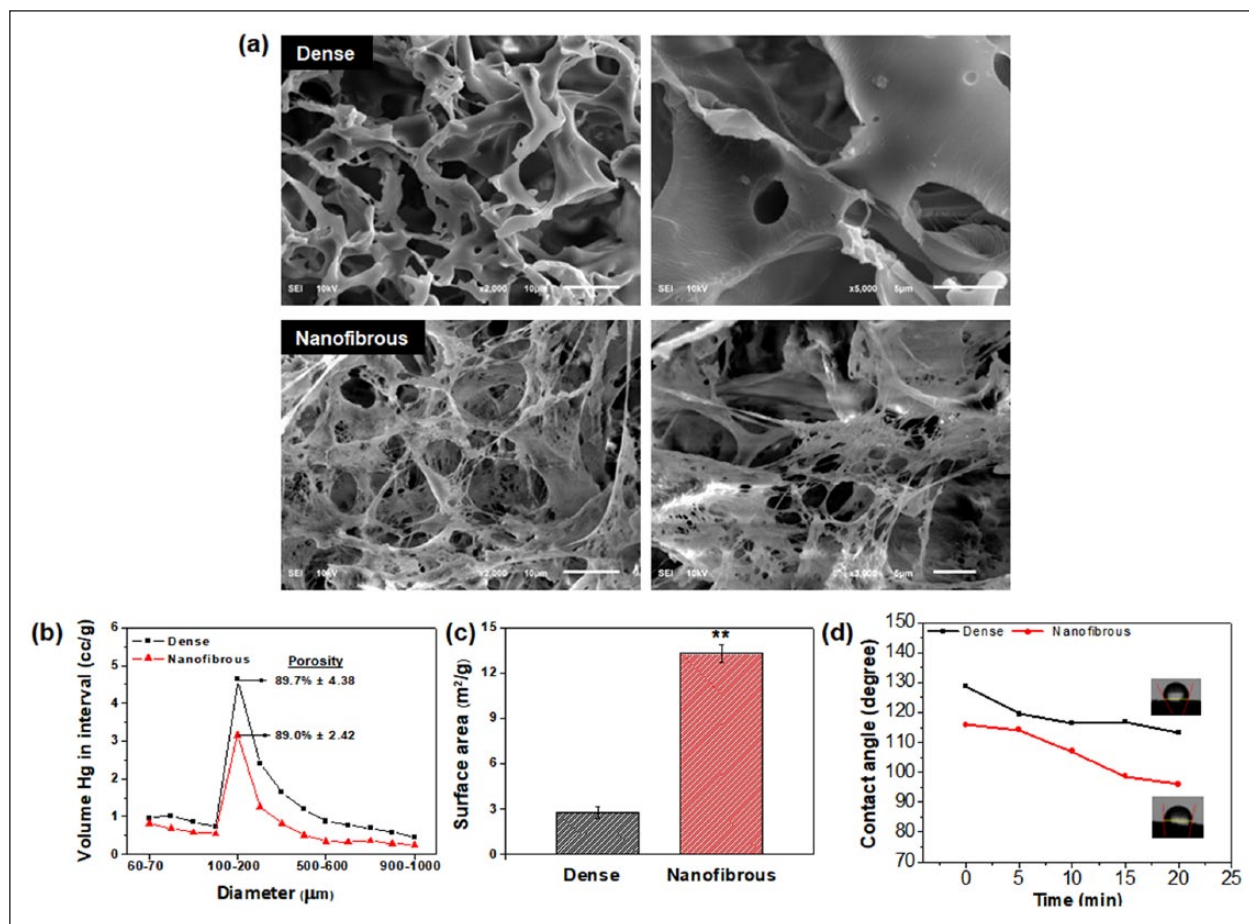
Figure 1. Characteristics of dense- and nanofibrous-surfaced 3D scaffolds: (a) SEM images showing the morphology of dense- and nanofibrous-surfaced porous scaffolds; (b) macro-porosity and pore size distribution, measured by a mercury intrusion porosimeter; (c) specific surface area, measured by a BET method; and (d) hydrophilicity, examined by a time-dependent change in water contact angle. Statistically significant difference indicated (**$p < 0.01$).

sites to water molecules, leading to an easier penetration of water into the pore channels.

Collectively, highly porous 3D scaffolds with a unique nanofibrous internal structure could be produced well, with a similar porosity and pore configuration to the conventional dense-surfaced counterpart. The nanofibrous structure significantly increased the surface area and water permeation of scaffolds. Of note, this behavior should play an important role in many biological interactions of scaffolds in body fluid or culture medium, with protein and cells, and thus possibly controlling the cell and tissue behaviors. While the nanofibrous scaffolds hold many physico-chemical merits that can allow active biological interactions, the mechanical properties are inferior to those of dense scaffolds due to very high porosities, which may limit the applications in load bearing parts.

CC responses

Rat primary CCs were used to examine the initial adhesion, proliferation, and the maintenance of CC phenotypes onto dense- and nanofibrous-surfaced scaffolds. The initial cell-to-scaffold adhesion was observed by the gene expression of integrin β1 which transmits signals between the extracellular matrix (ECM) and actin cytoskeleton (Figure 2(a)). The expression level of integrin β1 was analyzed at very initial time points (5, 30, 60, and 120 min). In the nanofibrous scaffold, the gene expression peaked as early as 30 min with a slight decrease with time, whereas in the dense scaffold the expression level appeared to increase more at later time point (highest at 120 min). It is thought that the integrin sensing of cells in the nanofibrous scaffold stimulated at very early time points (within an hour) changed to the responses of later adhesion molecules present intracellularly such as focal adhesion kinase.[36] The cell adhesion number onto nanofibrous scaffolds showed significantly higher value (~1.5 times) than that of dense scaffolds (Figure 2(b)). In addition, the cell viability on nanofibrous scaffolds as measured by a CCK assay was significantly higher than that on dense scaffolds (Figure 2(c)). We also observed that the cells grow well on both scaffolds with comparable cell growth kinetics (data not shown).
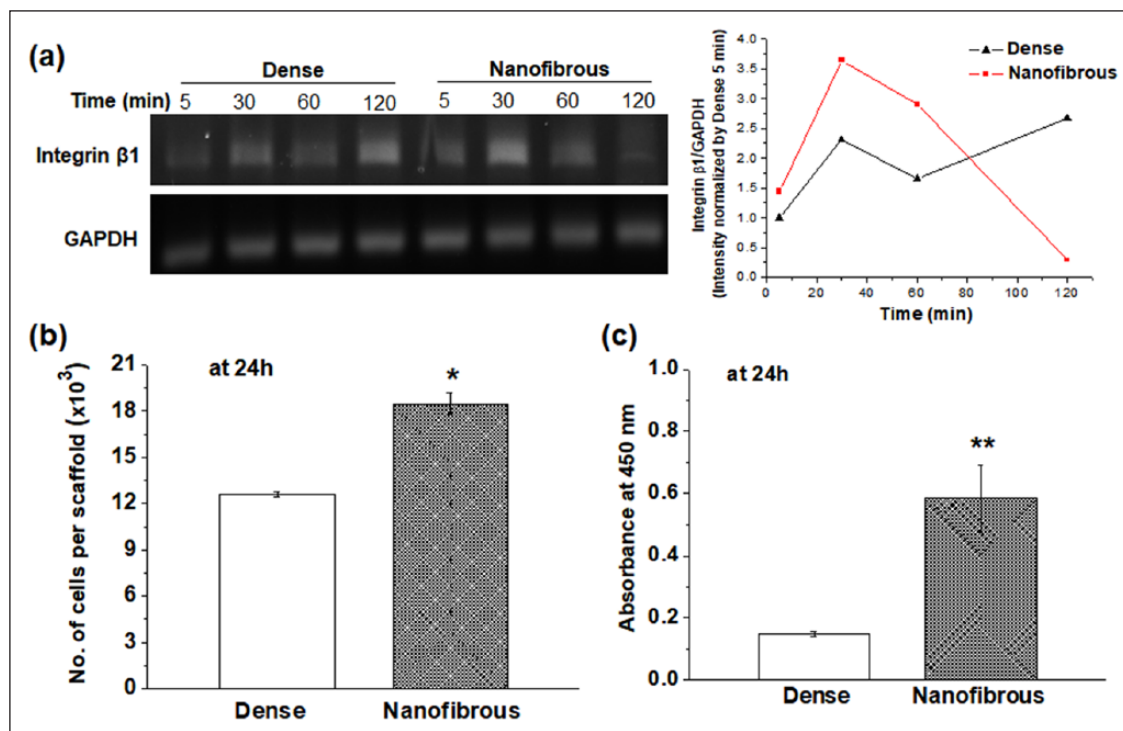
Figure 2. Chondrocyte adhesion compared between dense- and nanofibrous-surfaced scaffolds: (a) expression of integrin β1 by RT-PCR at 0, 30, 60, and 120 min, and the intensity quantified; (b) cell adhesion number; and (c) CCK viability at 24 h. Statistically significant difference noted ($*p < 0.05$; $**p < 0.01$; $n = 3$).

It is considered that the higher surface area of nanofibrous scaffolds could provide increased cellular adhesion sites to cells. This cell adhesion event, significantly enhanced in the nanofibrous scaffolds, can alter the subsequent cellular behaviors such as increased cell spreading and early differentiation, which has been reported to be detrimental to the maintenance of the chondrogenic phenotypes.[29,37–39]

Based on the cell-to-scaffold interaction results, the dense scaffolds are thought to offer more cell-to-cell interactions with respect to the nanofibrous scaffolds. The cell-to-cell interactions of CCs were examined by the morphological change and the Col II expression. For more accurate observation of the surface-nanostructure-dependent cellular interactions, the scaffolds were prepared in a flat membrane type which led to a development of morphology with less pronounced macropore channels but more contrasted dense or nanostructured surface topology (as provided in Figure 3(a)). The CCs cultured for 7 days showed clearly different behaviors. On the dense sample, the CCs were present unevenly, showing an irregular pattern-like circular arrangement of cell aggregates, whereas the cells on nanofibrous sample were distributed more evenly without an aggregation, based on optical microscopic images (Figure 3(b)). A closer examination under a confocal microscope revealed that the cells on the dense sample were closely packed with limited cytoskeletal

process, whereas those on the nanofibrous sample were highly extensive and presented minimal aggregation. The micro-mass morphology of the aggregated CCs observed on the dense scaffolds was similar to that found in native cartilage tissues.[40] This morphological development of CCs is closely related to the maintenance of CC phenotype and the maturation into a cartilage-like tissue. While the cell numbers counted in per field image were comparable on both surfaces, the cells on a dense surface were less homogeneous in a more aggregated form (Figure 3(c)). Of note, the intensity of Col II was significantly higher (~7 times) on the dense surface than on the nanofibrous surface (Figure 3(d)). Col II is considered as a representative marker of cell-to-cell contact of CCs. The collective results demonstrate that the dense scaffolds are able to enhance the cell-to-cell interactions at the cost of cell–matrix adhesions, which leads to form round-shaped cells with few actin filaments and ultimately the development of micromass cellular constructs.

Next, the expression of genes related to CC phenotype, such as SOX-9, Col II, and Aggrecan, were examined at days 7 and 14 by reverse transcription polymerase chain reaction (RT-PCR) (Figure 4(a)). All the genes were expressed more on the dense scaffolds than on the nanofibrous scaffolds, particularly at day 14. The most notable expression was found in Aggrecan, in which the dense scaffolds showed ~35 times of upregulation of the gene at day
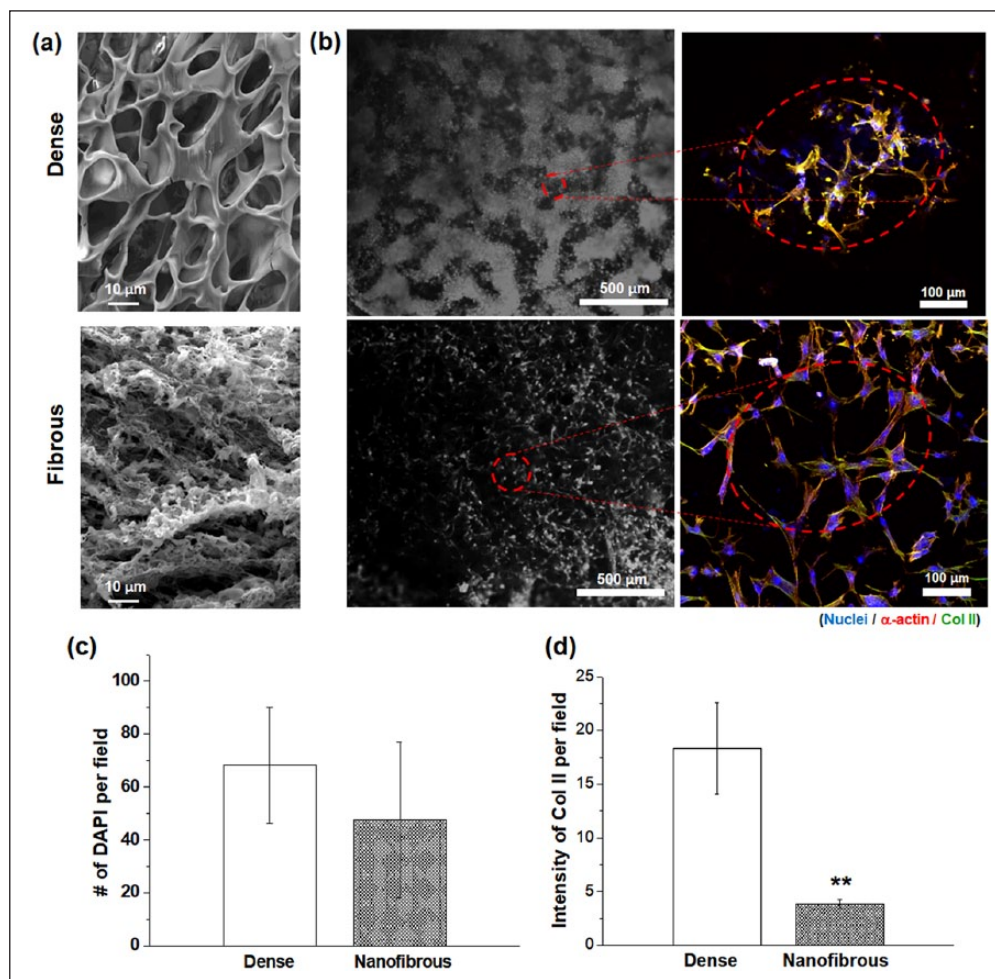
Figure 3. Cell-to-cell interaction assays compared between dense- and nanofibrous-surfaced scaffolds: (a) SEM morphological difference of dense- or nanofibrous-surfaced matrices used for the test; (b) representative CLSM images of immuno-stained cells at day 7 (blue: nuclei, red: α-actins, and green: Col II); (c) DAPI-stained nuclei number; and (d) Col II expression intensity, assayed from CLSM images.
Statistically significant difference noted (**$p < 0.01$; $n = 3$).

14 with respect to the nanofibrous scaffolds. While the SOX-9 and Col II are known as transcription factors expressed at relatively early stages mainly associated with the maintenance of the CCs,[41,42] the Aggrecan is produced relatively at later stages and considered as a major proteoglycan in cartilage ECM. While the Aggrecan expression is indicative of increased cell-to-cell interactions, it is also involved in the cell-to-ECM molecular interactions in cartilage due to its ability to bind hyaluronan.[43] Therefore, the expression of a substantial level of Aggrecan by the cells during the culture of 14 days on the dense-surfaced scaffolds suggested the possible functional development (i.e. cartilage-like ECM synthesis) of the cellular constructs. We further analyzed the production of a key cartilage matrix molecule GAG, by means of staining the cells with Alcian blue after 14 and 21 days culturing (Figure 4(b)). The cellular constructs cultured on dense-surface scaffolds revealed much darker blue color stains than those on the nanofibrous

scaffolds at both culture periods, thereby presenting significantly higher GAG production. The quantification result of the Alcian blue dye amount showed higher levels on the dense scaffolds than on the nanofibrous scaffolds. This is a clear indication that the CCs cultured on the dense-surface scaffolds become more functional to synthesis abundant GAG molecule, thus implying more potential for the cartilage regeneration when compared to the cells cultured on the nanofibrous scaffolds.

Collectively, we demonstrated that the CCs cultured on the nanofibrous-surfaced scaffolds were shown to exhibit lower levels of CC phenotypes and cartilage functionality than those on dense-surface scaffolds. The major reason is that the nanofibrous scaffolds provide a unique nano-topological feature where cells can recognize easily the underlying matrix through binding motifs; simultaneously, they are blocked to achieve more cell-to-cell contacts and the cellular aggregation, which is an
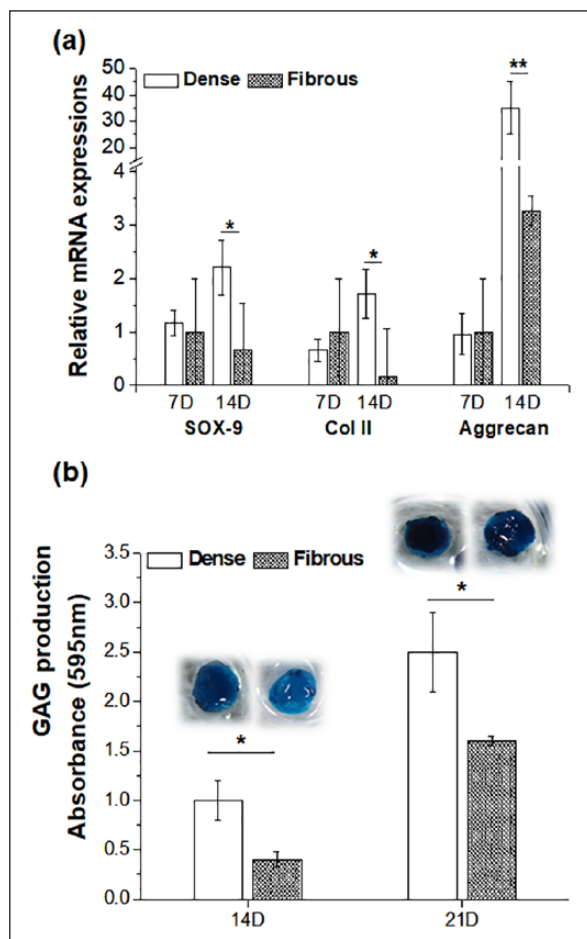
Figure 4. Maintenance of chondrocyte phenotypes differed in two types of scaffolds: (a) expression of chondrocyte-related genes, SOX-9, Col II, and Aggrecan, by qRT-PCR at 7 and 14 days and (b) GAG production as quantified by the Alcian blue stain assay (inset images showing Alcian blue–stained samples).
Statistically significant difference noted (*$p < 0.05$; **$p < 0.01$; $n = 3$).

essential step for the maintenance of CC phenotypes and functional development into a cartilage-like tissue. In fact, some previous studies have focused on the fibrous matrices prepared by electrospinning for the cartilage regeneration purposes.[44] The nanofibers made of poly(ε-caprolactone) were tuned to have different pore sizes ($1.2 \pm 0.2\,\mu m^2$ vs $90 \pm 10\,\mu m^2$), and the MSCs were cultured to differentiate into CCs. In the study, large pored nanofibers ($90 \pm 10\,\mu m^2$) were shown to support the chondrogenesis better by driving more cell–cell condensation, when compared with small pored ones ($1.2 \pm 0.2\,\mu m^2$). The large pores were shown to enhance the chondrogenesis through enhanced cell–cell gap junctions with decreased cell–matrix interactions.[45] Moreover, some previous studies reported that microfibers, compared with nanofibers, could better support the MSCs differentiation to CCs,[46,47] sharing some common

phenomenon with this study. Therefore, modulating the underlying matrices and scaffolds to favor cellular aggregation is considered as a key design strategy for CC culture and cartilage engineering.

MSC responses and the osteogenic stimulation

After assessment with CCs, the MSCs were then used to examine their interactions with two different types of scaffolds, including cell adhesion, growth, and osteogenic differentiation. Representative CLSM images visualized the morphology of cells at 4 h of adhesion. Compared to dense scaffolds, the nanofibrous scaffolds showed more cells and better spreading of them (Figure 5(a)). The cell adhesion recorded up to 16 h showed significantly higher levels on nanofibrous scaffolds than on dense scaffolds, particularly until 4 h, by a difference of ~3 times, suggesting the nanofibrous scaffolds accelerated the adhesion events of MSCs (Figure 5(b)). The cell proliferation rate measured up to 14 days showed to be similar between the two scaffolds (Supplemental Figure S1).

The osteogenesis of the MSCs was then identified by the expression of some key osteogenic proteins, for example, RUNX2, BSP, and OPN, by the western blot (Figure 6). The band intensities were also quantified. The relatively initial osteogenic marker, RUNX2, was expressed at significantly higher level on the fibrous scaffolds compared to the dense scaffolds at both 7 and 14 days. This trend was observed also for the relatively late osteogenic markers, BSP and OPN. A previous study has also demonstrated that MSCs were stimulated to differentiate into an osteogenic lineage upon nanostructured substrates, such as nanofibrillar structures, and the change in their cytoskeleton distribution had profound effect on their gene expression and protein expression and committed them to an osteogenic lineage.[48] The nano-patterned structure that could allow higher filopodia activity of MSCs has been considered as the main reason for the enhancement of osteogenic activity with respect to the flat surfaces.[49] The mineralization of the osteogenic committed cells was finally examined thorough the calcium deposition (Figure 7). The ARS staining showed much darker red color on the nanofibrous scaffolds compared to that on the dense scaffolds. When quantified, the difference was as high as six times.

Design strategy and concluding remark

Here, we successfully engineered 3D biopolymer scaffolds with two distinct surface morphologies, presenting dense and nanofibrous structures. While the dense scaffolds were effective for aggregating CCs and helping their maintenance of chondrogenic phenotypes, the nanofibrous morphology triggered adhesion events through cell–matrix interactions,
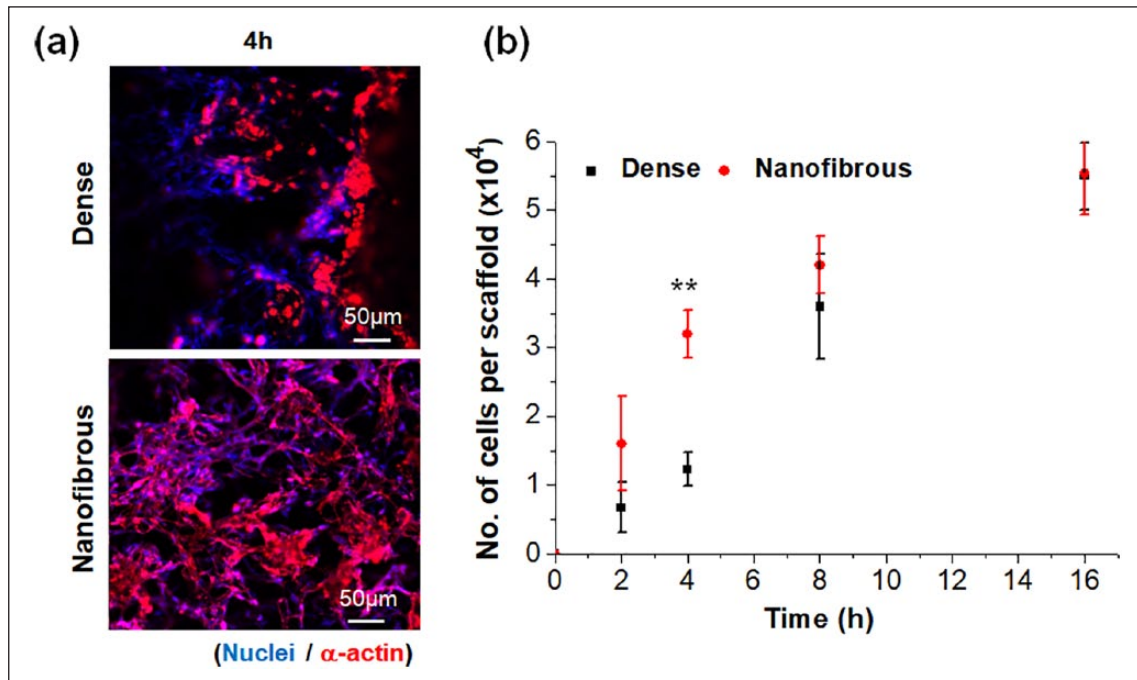
Figure 5. MSCs adhesion to dense- or nanofibrous-surfaced 3D scaffolds: (a) representative CLSM images of immuno-stained cells at 4 h (blue: nuclei, red: α-actins) and (b) cell adhesion number measured at various initial time points. Negative controls not shown. Statistically significant difference noted (*$p < 0.05$; **$p < 0.01$; $n = 3$).
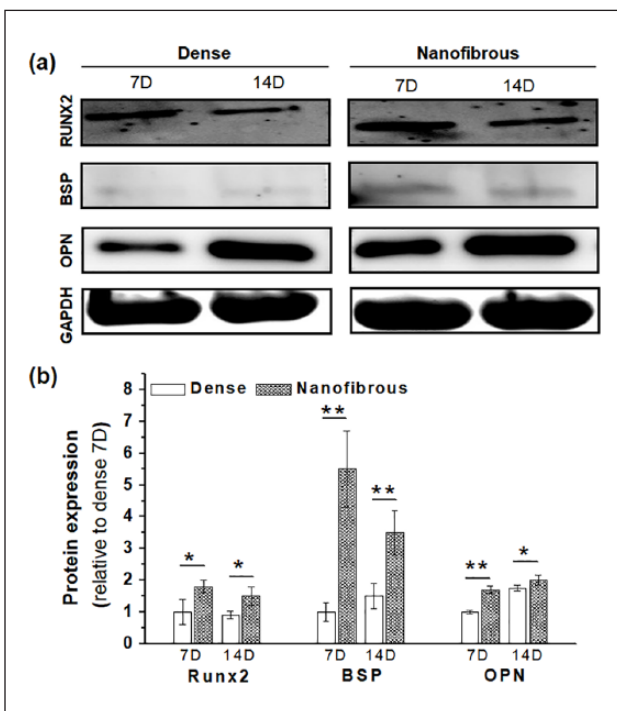

Figure 6. Osteogenic differentiation of MSCs differed in dense- and nanofibrous-surfaced scaffolds: (a) osteogenic protein expressions (OPN, RUNX2, and BSP), analyzed by western blot at 7 and 14 days and (b) the intensities quantified by ImageJ (data normalized to a group Dense 7D).
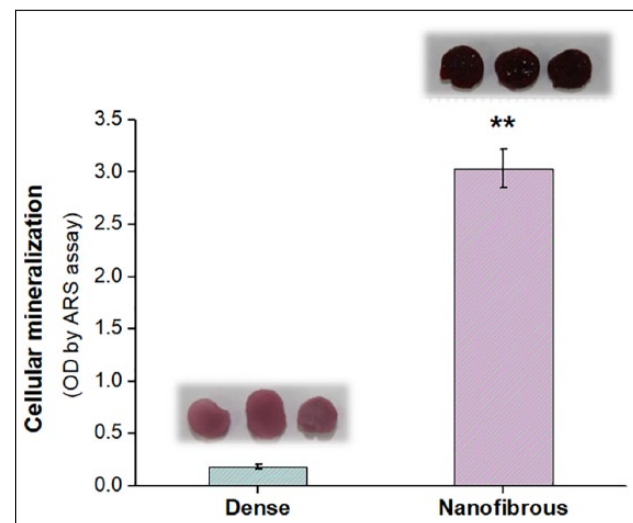Statistically significant difference noted (*$p < 0.05$; **$p < 0.01$; $n = 3$).

Figure 7. Mineralization of MSCs: ARS assay measured at 28 days, showing significantly higher level in nanofibrous scaffold (**$p < 0.01$; $n = 3$). Stained images are also attached.

downregulating chondrogenic preservation. On the contrary, the significant stimulation of adhesion events by the nanofibrous scaffolds was highly helpful for the MSCs to commit an osteogenic lineage, with the expression of related proteins and calcified nodules higher than those by the dense scaffolds. This reflects the reciprocal relationship between cell–cell interactions and cell–matrix interactions that are selectively
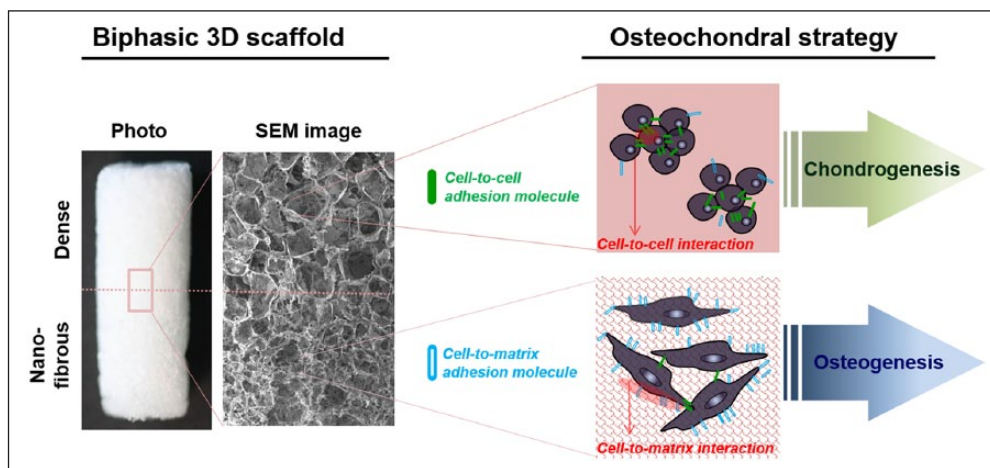
Figure 8. Schematic illustration of the design strategy for osteochondral engineering: Biphasic scaffolds can be designed based on the differential cellular responses on dense and nanofibrous surface.

favorable depending on the type of cells, that is, cell–cell interactions favored for CCs versus cell–matrix interactions for MSCs, which results from the different matrix conditions provided by the different surface nanostructures.

Therefore, as depicted in Figure 8, the nanofibrous and dense parts can be optimally designed to become an osteochondral biphasic scaffold. A merited aspect is that the process introduced in the preparation of the biphasic scaffolds (i.e. integrative molding a biphasic scaffold in one pot from two different solutions) is easy to control the parameters of scaffolds (dimension, pore size, composition, etc.). Through this method, further works—optimizing pore sizes (larger for osteo and smaller for chondro) or allowing more gradient structures (multiphasic)—will be of value to follow. Moreover, in vivo studies in osteochondral models using the optimally designed biphasic scaffolds may be needed to confirm the potential prior to find a clinical availability. This work demonstrates the differential osteogenic and chondrogenic responses to the underlying surface morphological conditions in a 3D scaffold system, offering a future strategy to design of the osteochondral scaffolds.

Supplemental material

Supplemental material for this article is available online.

ORCID iD

Hae-Won Kim https://orcid.org/0000-0001-6400-6100

References

1. Seo S-J, Mahapatra C, Singh RK, et al. Strategies for osteochondral repair: focus on scaffolds. *J Tissue Eng* 2014; 5: 2041731414541850.
2. Sherman SL, Garrity J, Bauer K, et al. Fresh osteochondral allograft transplantation for the knee: current concepts. *J Am Acad Orthop Sur* 2014; 22(2): 121–133.
3. Zengerink M, Struijs PA, Tol J, et al. Treatment of osteochondral lesions of the talus: a systematic review. *Knee Surg Sport Tr A* 2010; 18(2): 238–246.
4. Yucekul Ozdil D, Kutlu NH, et al. Tri-layered composite plug for the repair of osteochondral defects: in vivo study in sheep. *J Tissue Eng* 2017; 8: 2041731417697500.
5. Levingstone TJ, Thompson E, Matsiko A, et al. Multi-layered collagen-based scaffolds for osteochondral defect repair in rabbits. *Acta Biomater* 2016; 32: 149–160.
6. Temenoff JS and Mikos AG. Review: tissue engineering for regeneration of articular cartilage. *Biomaterials* 2000; 21(5): 431–440.
7. Nooeaid P, Salih V, Beier JP, et al. Osteochondral tissue engineering: scaffolds, stem cells and applications. *J Cell Mol Med* 2012; 16(10): 2247–2270.
8. von Bomhard A, Faust J, Elsaesser AF, et al. Impact of expansion and redifferentiation under hypothermia on chondrogenic capacity of cultured human septal chondrocytes. *J Tissue Eng* 2017; 8: 2041731417732655.
9. Donnelly H, Smith CA, Sweeten PE, et al. Bone and cartilage differentiation of a single stem cell population

driven by material interface. *J Tissue Eng* 2017; 8: 2041 731417705615.

10. Sancho-Tello M, Martorell S, Mata Roig M, et al. Human platelet-rich plasma improves the nesting and differentiation of human chondrocytes cultured in stabilized porous chitosan scaffolds. *J Tissue Eng* 2017; 8: 2041731417697545.

11. Jin G-Z, Kim J-J, Park J-H, et al. Biphasic nanofibrous constructs with seeded cell layers for osteochondral repair. *Tissue Eng Pt C: Meth* 2014; 20(11): 895–904.

12. Saha S, Kundu B, Kirkham J, et al. Osteochondral tissue engineering in vivo: a comparative study using layered silk fibroin scaffolds from mulberry and nonmulberry silkworms. *PLoS ONE* 2013; 8(11): e80004.

13. Das S, Pati F, Chameettachal S, et al. Enhanced redifferentiation of chondrocytes on microperiodic silk/gelatin scaffolds: toward tailor-made tissue engineering. *Biomacromolecules* 2013; 14(2): 311–321.

14. Maehara H, Sotome S, Yoshii T, et al. Repair of large osteochondral defects in rabbits using porous hydroxyapatite/collagen (HAp/Col) and fibroblast growth factor-2 (FGF-2). *J Orthop Res* 2010; 28(5): 677–686.

15. Oliveira JM, Rodrigues MT, Silva SS, et al. Novel hydroxyapatite/chitosan bilayered scaffold for osteochondral tissue-engineering applications: scaffold design and its performance when seeded with goat bone marrow stromal cells. *Biomaterials* 2006; 27(36): 6123–6137.

16. Yu H-S, Won J-E, Jin G-Z, et al. Construction of mesenchymal stem cell-containing collagen gel with a macrochanneled polycaprolactone scaffold and the flow perfusion culturing for bone tissue engineering. *Biores Open Access* 2012; 1(3): 124–136.

17. Lee JH, Park J-H, Yun Y-R, et al. Tethering bi-functional protein onto mineralized polymer scaffolds to regulate mesenchymal stem cell behaviors for bone regeneration. *J Mater Chem B* 2013; 1(21): 2731–2741.

18. Singh RK, Patel KD, Lee JH, et al. Potential of magnetic nanofiber scaffolds with mechanical and biological properties applicable for bone regeneration. *PLoS ONE* 2014; 9(4): e91584.

19. Tacchetti C, Tavella S, Dozin B, et al. Cell condensation in chondrogenic differentiation. *Exp Cell Res* 1992; 200(1): 26–33.

20. Bosnakovski D, Mizuno M, Kim G, et al. Chondrogenic differentiation of bovine bone marrow mesenchymal stem cells in pellet cultural system. *Exp Hematol* 2004; 32(5): 502–509.

21. Estes BT, Diekman BO, Gimble JM, et al. Isolation of adipose-derived stem cells and their induction to a chondrogenic phenotype. *Nat Protoc* 2010; 5(7): 1294–1311.

22. Legg K. Stem cells: chondrogenesis induced from human embryonic stem cells. *Nat Rev Rheumatol* 2010; 6(2): 66–66.

23. Occhetta P, Centola M, Tonnarelli B, et al. High-throughput microfluidic platform for 3D cultures of mesenchymal stem cells, towards engineering developmental processes. *Sci Rep* 2015; 5: 10288.

24. Foster NC, Henstock JR, Reinwald Y, et al. Dynamic 3D culture: models of chondrogenesis and endochondral ossification. *Birth Defects Res C* 2015; 105(1): 19–33.

25. Baker BM and Chen CS. Deconstructing the third dimension—how 3D culture microenvironments alter cellular cues. *J Cell Sci* 2012; 125(13): 3015–3024.

26. Tanaka Y, Yamaoka H, Nishizawa S, et al. The optimization of porous polymeric scaffolds for chondrocyte/atelocollagen based tissue-engineered cartilage. *Biomaterials* 2010; 31(16): 4506–4516.

27. Matsiko A, Gleeson JP and O'Brien FJ. Scaffold mean pore size influences mesenchymal stem cell chondrogenic differentiation and matrix deposition. *Tissue Eng Pt A* 2014; 21(3–4): 486–497.

28. Wu Y, Yang Z, Law JBK, et al. The combined effect of substrate stiffness and surface topography on chondrogenic differentiation of mesenchymal stem cells. *Tissue Eng Pt A* 2017; 23: 43–54.

29. Cao B, Peng R, Li Z, et al. Effects of spreading areas and aspect ratios of single cells on dedifferentiation of chondrocytes. *Biomaterials* 2014; 35(25): 6871–6881.

30. Kim J-J, Bang S-H, El-Fiqi A, et al. Fabrication of nanofibrous macroporous scaffolds of poly(lactic acid) incorporating bioactive glass nanoparticles by camphene-assisted phase separation. *Mater Chem Phys* 2014; 143(3): 1092–1101.

31. Kim J-J, El-Fiqi A and Kim H-W. Synergetic cues of bioactive nanoparticles and nanofibrous structure in bone scaffolds to stimulate osteogenesis and angiogenesis. *ACS Appl Mater Inter* 2017; 9(3): 2059–2073.

32. Gartland A, Mechler J, Mason-Savas A, et al. In vitro chondrocyte differentiation using costochondral chondrocytes as a source of primary rat chondrocyte cultures: an improved isolation and cryopreservation method. *Bone* 2005; 37(4): 530–544.

33. Lee JH, Lee J-Y, Yang SH, et al. Carbon nanotube-collagen three-dimensional culture of mesenchymal stem cells promotes expression of neural phenotypes and secretion of neurotrophic factors. *Acta Biomater* 2014; 10(10): 4425–4436.

34. Mahapatra C, Jin GZ and Kim HW. Alginate-hyaluronic acid-collagen composite hydrogel favorable for the culture of chondrocytes and their phenotype maintenance. *Tissue Eng Regen Med* 2016; 13(5): 538–546.

35. Miao X and Sun D. Graded/gradient porous biomaterials. *Materials* 2009; 3(1): 26–47.

36. Böttcher RT, Stremmel C, Meves A, et al. Sorting nexin 17 prevents lysosomal degradation of β1 integrins by binding to the β1-integrin tail. *Nat Cell Biol* 2012; 14(6): 584–592.

37. Li Z, Cao B, Wang X, et al. Effects of RGD nanospacing on chondrogenic differentiation of mesenchymal stem cells. *J Mater Chem B* 2015; 3(26): 5197–5209.

38. Garcia-Giralt N, Izquierdo R, Nogués X, et al. A porous PCL scaffold promotes the human chondrocytes redifferentiation and hyaline-specific extracellular matrix protein synthesis. *J Biomed Mater Res A* 2008; 85(4): 1082–1089.

39. Kim D, Choi B, Song J, et al. TiO_2 nanotube stimulate chondrogenic differentiation of limb mesenchymal cells by modulating focal activity. *Exp Mol Med* 2011; 43: 455–461.

40. Murphy MK, Huey DJ, Reimer AJ, et al. Enhancing post-expansion chondrogenic potential of costochondral cells in self-assembled neocartilage. *PLoS ONE* 2013; 8(2): e56983.

41. Mori-Akiyama Y, Akiyama H, Rowitch DH, et al. Sox9 is required for determination of the chondrogenic cell lineage in the cranial neural crest. *P Natl Acad Sci USA* 2003; 100(16): 9360–9365.

42. Bell DM, Leung KKH, Wheatley SC, et al. Sox9 directly regulates the type-II collagen gene. *Nat Genet* 1997; 16(2): 174–178.

43. Kiani C, Liwen C, Wu YJ, et al. Structure and function of aggrecan. *Cell Res* 2002; 12(1): 19–32.

44. Allison CB and Rocky ST. Fiber diameter and seeding density influence chondrogenic differentiation of mesenchymal stem cells seeded on electrospun poly(ε-caprolactone) scaffolds. *Biomed Mater* 2015; 10(1): 015018.

45. de Windt TS, Saris DBF, Slaper-Cortenbach ICM, et al. Direct cell-cell contact with chondrocytes is a key mechanism in multipotent mesenchymal stromal cell-mediated chondrogenesis. *Tissue Eng Pt A* 2015; 21: 2536–2547.

46. Jingjing Z, Yingnan W, Tanushree T, et al. The influence of scaffold microstructure on chondrogenic differentiation of mesenchymal stem cells. *Biomed Mater* 2014; 9(3): 035011.

47. Ragetly GR, Griffon DJ, Lee H-B, et al. Effect of chitosan scaffold microstructure on mesenchymal stem cell chondrogenesis. *Acta Biomater* 2010; 6(4): 1430–1436.

48. Singh RK, Jin G-Z, Mahapatra C, et al. Mesoporous silica-layered biopolymer hybrid nanofibrous scaffold: a novel nanobiomatrix platform for therapeutics delivery and bone regeneration. *ACS Appl Mater Inter* 2015; 7(15): 8088–8098.

49. El-Fiqi A, Kim J-H and Kim H-W. Osteoinductive fibrous scaffolds of biopolymer/mesoporous bioactive glass nanocarriers with excellent bioactivity and long-term delivery of osteogenic drug. *ACS Appl Mater Inter* 2015; 7(2): 1140–1152.